Sub-cycle Oscillations in Virtual States Brought to Light

(Supplementary Information)

Michael Chini[1], Xiaowei Wang[1,2], Yan Cheng[1], Yi Wu[1], Di Zhao[3,4],

Dmitry A. Telnov[3,5], Shih-I Chu[3,6], and Zenghu Chang[1]*

[1]*CREOL and Department of Physics, University of Central Florida, Orlando, FL 32816, USA*

[2] *Department of Physics, National University of Defense Technology, Changsha, Hunan 410073, China*

[3]*Department of Chemistry, University of Kansas, Lawrence, KS 66045, USA*

[4]*Department of Applied Physics, Xi'an Jiaotong University, Xi'an, Shanxi 710049, China*

[5]*Department of Physics, St. Petersburg State University, St. Petersburg 198504, Russia*

[6]*Center for Quantum Science and Engineering, National Taiwan University, Taipei 10617, Taiwan*

*E-mail: Zenghu.Chang@ucf.edu

Classification of two-color multi-photon absorption structures

When the isolated attosecond pulse is absorbed by the helium gas in the presence of a few-cycle near infrared (NIR) laser field, we observe new absorption features, which shift in energy as the delay is scanned from zero to -25 *fs*, and which oscillate in absorption strength in the region of temporal overlap near zero delay. We can consider the absorption at large negative delays to be related to a "sequential" process, where the XUV photons in the vicinity of the 1s2p energy level are absorbed to a transient "virtual" excited state, and the delayed NIR pulse later excites the electron to a 1s*nl* state (*l* = *s*, *d*) which cannot be populated by the XUV pulse alone due to dipole selection rules. The experimental data in Fig. 3a in the main text is difficult to

interpret without the aid of theoretical simulations, due to the high intensity and broad bandwidth of the dressing laser field. With lower dressing laser intensities, the broadening of the absorption lines is substantially smaller (see Fig. 1c in the main text), and the interpretation of the data is somewhat simplified. Furthermore, the large AC Stark and ponderomotive energy level shifts are suppressed, allowing us to separate the contributions of various 1s*nl* states to the virtual state absorption lines. Figs. 1a and b show the measured absorbance in the vicinity of the 1s2p energy level for lower dressing laser intensities of 7×10^{11} W/cm^2 and 5×10^{12} W/cm^2, respectively, with features corresponding to the virtual states labeled.

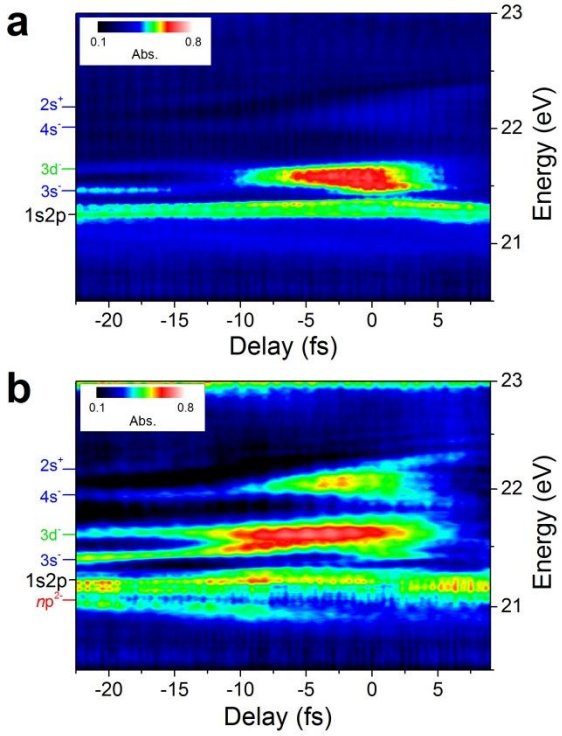

Fig. 1 | Two-color multi-photon absorption in time-resolved absorption. The absorption in the vicinity of the 1s2p state at lower dressing laser intensities of **a,** 7×10^{11} W/cm^2 and **b,** 5×10^{12} W/cm^2 allow for experimental identification of the virtual states appearing in the laser-dressed absorption.

While the features observed near zero delay are rather broad and appear to result from the contribution of several Stark-shifted 1s*n*s and 1s*n*d states, the absorption features can be traced

back to large negative delays, where the absorption lines become relatively narrow and are not affected by AC Stark shifts. We observe the $3s^-$ absorption feature at an energy of E_{1s3s} - 1.5 eV = 21.4 eV, the $3d^-$ absorption feature at an energy of E_{1s3d} - 1.5 eV = 21.6 eV, the $4s^-$ absorption feature at an energy of E_{1s4s} - 1.7 eV = 22.0 eV, the $2s^+$ absorption feature at an energy of E_{1s2s} + 1.6 eV = 22.2 eV, and the np^{2-} absorption feature at an energy of E_{1snp} - 2×1.7 eV = 21.0 eV (for example, E_{1s6p} = 24.21 eV and higher-lying states). While the energy differences between the transient state absorption features and the field-free final states all lie within the bandwidth of the few-cycle laser field, it is not immediately clear why the energy differences are not consistent for all states.

The classification of the absorption peaks can be confirmed by solution of the time-dependent Schrödinger equation. Whereas the simulations shown in Figures 2b and 4a in the main text result from solution of the coupled equations and can therefore consider only a limited number of excited states, here we fully consider the transient absorption of the XUV radiation by the helium atom in the presence of the NIR laser field. The XUV field is weak (~10^{10} W/cm^2) and can be treated as a perturbation. The NIR field, on the contrary, is regarded as weak only for the helium ground state. All excited states can be strongly perturbed by the field, resulting in substantial shifting and broadening of the energy levels. Since the duration of the NIR laser is much longer than that of the XUV pulse, we extend the non-Hermitian Floquet theory[1, 2] to describe the interaction of the atom with the NIR field nonperturbatively. The Floquet state is characterized by the complex quasienergy, with its real part reflecting the AC Stark shift of the atomic energy level in the laser field and the imaginary part equal to $-\Gamma/2$ where Γ is the decay rate of the atomic state in the external field. Then, the correction to the imaginary part of the quasienergy due to the XUV field is directly related to the absorption rate of XUV photons. The

N-photon absorption cross-section can be calculated as the *N*-photon absorption rate Γ divided by I^N, where *I* is the photon flux and *N* is the number of photons absorbed[1].

We describe the helium atom by an accurate model potential which reproduces the ground, singly-excited, and Rydberg states to a high precision[3]. To calculate the XUV photoabsorption cross section, we extend the non-Hermitian Floquet perturbation theory[4] to the current XUV+NIR field transient absorption problem. First, we solve for the NIR-dressed atom wave functions non-perturbatively using the non-Hermitian Floquet theory[1, 2]. The Floquet wave function $\Psi_\varepsilon(\mathbf{r},t)$ is represented as a product of the quasienergy exponential factor and a time-periodic function $\psi_\varepsilon(\mathbf{r},t)$:

$$\Psi_\varepsilon(\mathbf{r},t) = \exp(-i\varepsilon t)\psi_\varepsilon(\mathbf{r},t). \quad (1)$$

All equations are given in atomic units unless otherwise noted. The time-periodic wave function $\psi_\varepsilon(\mathbf{r},t)$ is the eigenfunction of the Floquet Hamiltonian H, defined in the composite Hilbert space:

$$H\psi_\varepsilon(\mathbf{r},t) = \varepsilon\psi_\varepsilon(\mathbf{r},t), \quad (2)$$

$$H = H_0 + V_{NIR}(\mathbf{r},t) - i\frac{\partial}{\partial t}. \quad (3)$$

By employing the complex scaling transformation[1, 2] of the spatial coordinates and Fourier series expansion of the periodic function $\psi_\varepsilon(\mathbf{r},t)$ in the time domain, Eq. (2) is converted into a time-independent non-Hermitian Floquet matrix eigenvalue problem, and one can obtain a set of complex quasienergies and corresponding left and right eigenvectors which possess the property of biorthogonality. Then we apply the perturbation theory with respect to the XUV field $V_{XUV}(\mathbf{r},t)$. To analyze the frequency-resolved absorption of the XUV field by the laser-dressed atom, we consider a monochromatic XUV field with the frequency Ω:

$$V_{XUV}(\mathbf{r},t) = V_{+}(\mathbf{r})\exp(-i\Omega t) + V_{-}(\mathbf{r})\exp(+i\Omega t). \quad (4)$$

The eigenvalue problem to solve is now

$$\left[H + V_{XUV}(\mathbf{r},t)\right]\psi_0(\mathbf{r},t) = \varepsilon_0\psi_0(\mathbf{r},t). \quad (5)$$

The wavefunction $\psi_0(\mathbf{r},t)$ and the eigenvalue ε_0 can be sought in the form of a series expansion in powers of the perturbation V_{XUV}:

$$\psi_0(\mathbf{r},t) = \psi_0^{(0)} + \psi_0^{(1)} + \psi_0^{(2)} + \ldots \quad (6)$$

$$\varepsilon_0 = \varepsilon_0^{(0)} + \varepsilon_0^{(1)} + \varepsilon_0^{(2)} + \ldots \quad (7)$$

Here $\psi_0^{(0)}$ and $\varepsilon_0^{(0)}$ are the unperturbed ground state eigenfunction and eigenvalue that satisfy Eq. (2). The first order correction to the quasienergy $\varepsilon_0^{(1)}$ vanishes due to parity restrictions if we neglect the dressing laser effect on the ground state of the helium atom. This approximation is well justified for the intensities of the NIR field used in the experiment. The second-order correction $\varepsilon_0^{(2)}$ can be represented as follows:

$$\varepsilon_0^{(2)} = \left\langle \psi_0^{(0)} \middle| V_{XUV} G V_{XUV} \middle| \psi_0^{(0)} \right\rangle, \quad (8)$$

where the reduced Green's function G is defined by the expansion on the basis of the unperturbed eigenfunctions $\psi_n^{(0)}$ of the Floquet Hamiltonian H:

$$G = \sum_{n\neq 0} \frac{\left|\psi_n^{(0)}\right\rangle\left\langle\psi_n^{(0)}\right|}{\varepsilon_n^{(0)} - \varepsilon_0^{(0)}}. \quad (9)$$

Finally, the laser-assisted photoabsorption cross-section σ at the frequency Ω is calculated as the decay rate (twice the absolute value of the imaginary part of the quasienergy) divided by the photon flux:

$$\sigma = \frac{16\pi}{c}\,\mathrm{Im}\left(\left\langle \psi_0^{(0)} \middle| V_{XUV} G V_{XUV} \middle| \psi_0^{(0)} \right\rangle\right). \quad (10)$$

Substituting the Green's function of Eq. (9) into Eq. (10), we obtain:

$$\sigma = \sum_{n \neq 0} \sigma_n \,, \tag{11}$$

with

$$\sigma_n = \frac{16\pi\Omega}{c} \mathrm{Im}\left(\frac{\left\langle \psi_0^{(0)} \middle| V_{XUV} \middle| \psi_n^{(0)} \right\rangle \left\langle \psi_n^{(0)} \middle| V_{XUV} \middle| \psi_0^{(0)} \right\rangle}{\varepsilon_n^{(0)} - \varepsilon_0^{(0)}} \right). \tag{12}$$

The quantity σ_n is the contribution of the excitation of the nth Floquet state to the total cross-section.

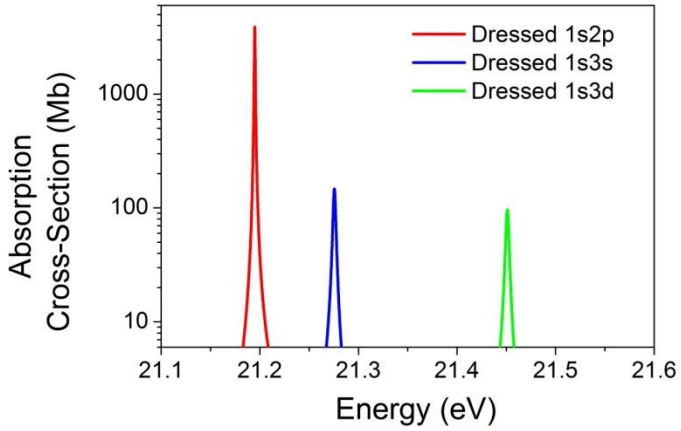

Fig. 2 | Contribution to the total cross-section of individual Floquet states. The 1s2p state (red) is the dominant contribution to the cross-section, while new absorption lines originating from the dressed 1s3s (blue) and 1s3d (green) appear with the addition of the laser. The dressing laser intensity was 1×10^{11} W/cm^2.

In Fig. 2, we show the individual contribution to the photoabsorption cross-section of the laser-dressed helium atom by the Floquet (or *dressed*) states originating from the 1s2p, 1s3s, and 1s3d atomic levels. The additional peaks which appear in the vicinity of the $1s^2$-1s2p absorption line have been identified as contributed from the excitation of the dressed 1s3s and 1s3d levels, respectively. An alternative method of identification of additional peaks in the cross section is

based on the calculation of the photoabsorption cross-section with atomic Hamiltonians which lack some of the energy levels:

$$H_0^{3d} = H_0 - E_{3d}|\psi_{3d}\rangle\langle\psi_{3d}|, \tag{13}$$

$$H_0^{3s3d} = H_0 - E_{3d}|\psi_{3d}\rangle\langle\psi_{3d}| - E_{3s}|\psi_{3s}\rangle\langle\psi_{3s}|. \tag{14}$$

Here the Hamiltonian H_0^{3d} does not have the 1s3d energy level, while both 1s3d and 1s3s energy levels are absent in the Hamiltonian H_0^{3s3d}. Comparing the results of the calculations with the Hamiltonians H_0, H_0^{3d}, and H_0^{3s3d}, as shown in Fig. 2 for a dressing laser intensity of 1×10^{11} W/cm^2, one can unambiguously identify the origin of different absorption lines in the frequency range of interest. The low dressing laser intensity was chosen to minimize the effects of the AC Stark shifts, which are also modified by removing energy levels from the Hamiltonian. The main 1s2p absorption line is located approximately at 21.19 eV, while the additional 1s3s ($3s^-$) and 1s3d ($3d^-$) subpeaks are found at the photon energies of 21.27 and 21.53 eV, respectively. The line positions for the Hamiltonians H_0^{3d} and H_0^{3s3d} are slightly different because the interactions with the 1s3d (or both 1s3d and 1s3s) states, which also contribute to the AC Stark shift, are missing for these Hamiltonians. Generally it can be understood that such additional peaks arise due to excitation of other atomic levels by the combination of the XUV and NIR fields. The strongest peaks correspond to absorption of one XUV and one NIR photon.

Oscillatory Structures in the Time-Delay-Resolved Transition Probability

In the previous section, we have applied the non-Hermitian Floquet perturbation theory to the *monochromatic* XUV field. Here, we consider an isolated attosecond XUV pulse and discuss the dependence of the transition probabilities on the time delay between the XUV pulse and the

NIR field. We assume that the NIR field is monochromatic with the frequency ω_{NIR} and field strength F_{NIR}:

$$V_{NIR}(\mathbf{r},t) = zF_{NIR}\cos(\omega_0 t). \tag{15}$$

Here, linear polarization in the z-direction is assumed. For the XUV pulse, we adopt the Gaussian shape in time with the width τ_{XUV}, the central frequency ω_{XUV}, and the same polarization direction:

$$V_{XUV}(\mathbf{r},t) = zF_{XUV}\exp\left[-\frac{(t-\tau_D)^2}{\tau_{XUV}^{\ 2}}\right]\exp\left(-i\omega_{XUV}t\right). \tag{16}$$

Here, F_{XUV} is the peak field strength and τ_D is the time delay between the XUV pulse and the NIR field. The wave function $\Psi(\mathbf{r},t)$ of the electron subjected to the combination of the XUV and NIR fields can be expanded on the basis of the Floquet wave functions $\Psi_n^{(0)}(\mathbf{r},t) = \exp(-i\varepsilon_n^{(0)}t)\psi_n^{(0)}(\mathbf{r},t)$ defined by Eq. (1) in the NIR field only:

$$\Psi(\mathbf{r},t) = \sum_n C_n(t)\exp(-i\varepsilon_n^{(0)})\psi_n^{(0)}(\mathbf{r},t), \tag{17}$$

where the expansion coefficients $C_n(t)$ vary in time during the XUV pulse only. Before the XUV pulse, $C_n = \delta_{n0}$ (only one Floquet state corresponding to the initial atomic energy level is populated). After the XUV pulse, the coefficient C_n has the meaning of the transition amplitude to the nth Floquet state. Employing the first-order time-dependent perturbation theory with respect to V_{XUV}, the transition amplitude C_n can be expressed as follows:

$$C_n = i\int_{-\infty}^{\infty} dt\exp\left[i(\varepsilon_n^{(0)} - \varepsilon_0^{(0)})t\right]\left\langle\psi_n^{(0)}\middle|V_{XUV}\middle|\psi_0^{(0)}\right\rangle, \tag{18}$$

and the corresponding transition probability is obtained as the squared absolute value of C_n:

$$P_n = \left|C_n\right|^2 . \tag{19}$$

The time-periodic functions $\psi_n^{(0)}(\mathbf{r},t)$ can be expanded in a Fourier series:

$$\psi_n^{(0)}(\mathbf{r},t) = \sum_{m=-\infty}^{\infty} \exp(-im\omega_{NIR}t)\psi_{n,m}^{(0)}(\mathbf{r}) . \tag{20}$$

As we have already mentioned, the NIR field is weak enough that we can neglect the dressing of the ground state. Within this approximation,

$$\psi_0^{(0)}(\mathbf{r},t) \approx \psi_{0,0}^{(0)}(\mathbf{r}) . \tag{21}$$

Using Eqs. (20) and (16) in Eqs. (18) and (19), one obtains:

$$P_n = \pi(\tau_{XUV}F_{XUV})^2 \left| \sum_{m=-\infty}^{\infty} A_{n,m} \exp(im\omega_{NIR}\tau_D) \right|^2 , \tag{22}$$

$$A_{n,m} = \left\langle \psi_{n,m}^{(0)} \left| z \right| \psi_0^{(0)} \right\rangle \exp\left[-\frac{\tau_{XUV}^{\ 2}}{4} (\varepsilon_n^{(0)} + m\omega_{NIR} - \varepsilon_0^{(0)} - \omega_{XUV})^2 \right] . \tag{23}$$

Due to parity restrictions for the dipole matrix elements, the coefficients $A_{n,m}$ vanish for odd *m* if the final state has odd parity (such as 1s*n*p) and for even *m* if the final state has even parity (such as 1s*n*s and 1s*n*d). For this reason, the sum in Eq. (22) will contain either odd or even *m* contributions only. In any case, the probability P_n can be expanded in a Fourier series with the fundamental $2\omega_{NIR}$ equal to twice the frequency of the NIR field. Retaining the first few Fourier components, the expression for P_n can be written as:

$$\begin{aligned} P_n^{odd} \approx \pi(\tau_{XUV}F_{XUV})^2 \Big\{ & \left|A_{n,0}\right|^2 + \left|A_{n,2}\right|^2 + \left|A_{n,-2}\right|^2 + \left|A_{n,4}\right|^2 + \left|A_{n,-4}\right|^2 \\ & + 2\,\mathrm{Re}\Big[A_{n,0}A_{n,2}^* \exp(-i2\omega_{NIR}\tau_D) + A_{n,0}A_{n,-2}^* \exp(i2\omega_{NIR}\tau_D) \\ & + A_{n,0}A_{n,4}^* \exp(-i4\omega_{NIR}\tau_D) + A_{n,0}A_{n,-4}^* \exp(i4\omega_{NIR}\tau_D) \\ & + A_{n,2}A_{n,-2}^* \exp(i4\omega_{NIR}\tau_D) + A_{n,-2}A_{n,2}^* \exp(-i4\omega_{NIR}\tau_D) \Big] \Big\}, \end{aligned} \tag{24}$$

for the odd states, while for the even final states (such as 1s*n*s and 1s*n*d), it reads as:

$$P_n^{even} \approx \pi(\tau_{XUV} F_{XUV})^2 \Big\{ |A_{n,1}|^2 + |A_{n,-1}|^2 + |A_{n,3}|^2 + |A_{n,-3}|^2$$
$$+ 2\,\mathrm{Re}\big[A_{n,-1}A_{n,1}^* \exp(-i2\omega_{NIR}\tau_D) + A_{n,1}A_{n,-1}^* \exp(i2\omega_{NIR}\tau_D)$$
$$+ A_{n,-1}A_{n,-3}^* \exp(i2\omega_{NIR}\tau_D) + A_{n,1}A_{n,3}^* \exp(-i2\omega_{NIR}\tau_D)$$
$$+ A_{n,-1}A_{n,3}^* \exp(-i4\omega_{NIR}\tau_D) + A_{n,3}A_{n,-1}^* \exp(i4\omega_{NIR}\tau_D)\big]\Big\}. \qquad (25)$$

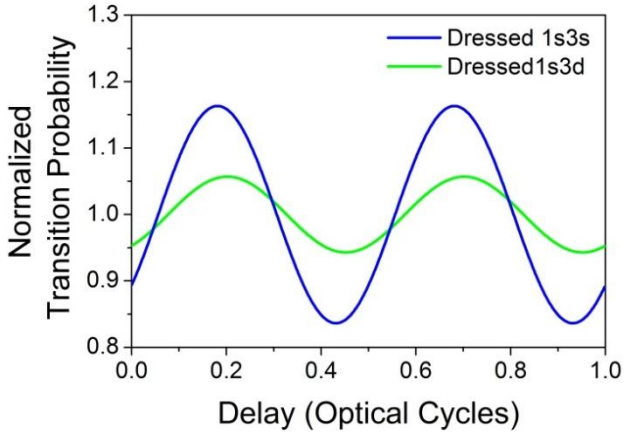

Fig. 3 | Normalized transition probability to dressed 1s*n*p states as a function of the time delay. The dressed 1s3s (blue) and 1s3d (green) states exhibit clear half-cycle periodicities.

Eqs. (24) and (25) suggest that the transition probability P_n oscillates as a function of the time delay τ_D between the XUV and NIR fields with twice the frequency of the NIR field and also contains higher-frequency contributions. For weak or moderate NIR fields, the largest coefficient $A_{n,m}$ is for m = 0; in the perturbative regime, this corresponds to the lowest order perturbation theory with respect to the NIR field. Increasing $|m|$ by one means also increasing the order of perturbation theory by one. Thus, the quarter-cycle ($4\,\omega_{NIR}$) oscillations for the odd final states, Eq. (24), can be obtained from the 2nd order perturbation term (m = ±2) in the

transition amplitude. These oscillations are therefore quite small and can be visible only because they appear on the satellite absorption line which is shifted by $2\,\omega_{NIR}$ from the main 1s*n*p line. In Fig. 3, we present the delay-dependent transition probabilities from the ground state to the *dressed* 1s3d and 1s3s states at the NIR intensity of 1×10^{11} W/cm^2.

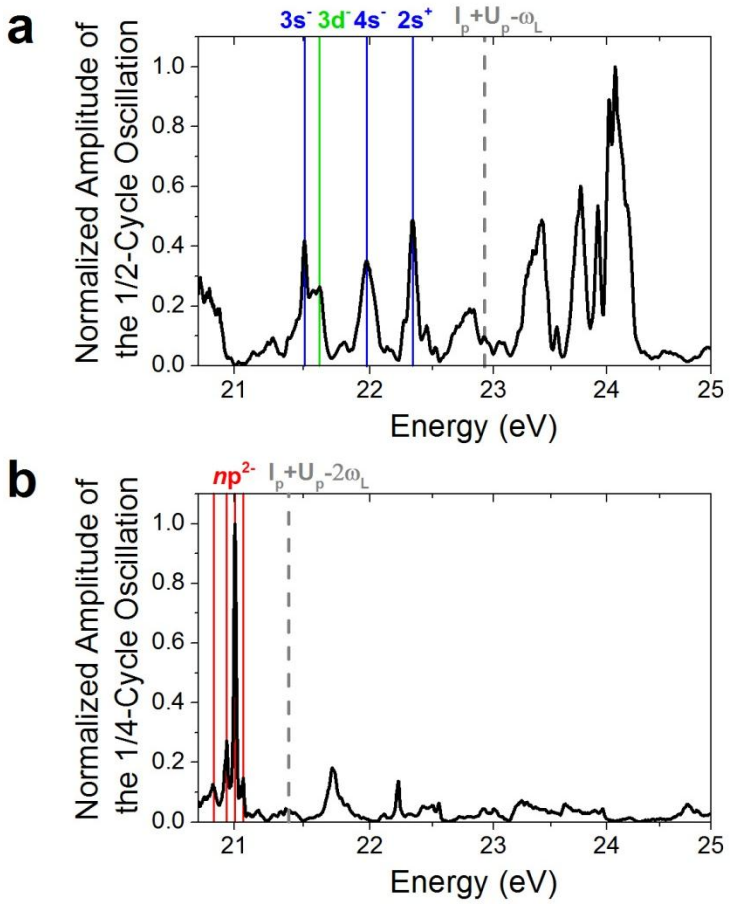

Fig. 4 | Classification of two- and three-photon absorption pathways and sub-cycle oscillations. a, Half-cycle oscillations corresponding to two-photon absorption pathways. The half-cycle oscillations indicate the first-order perturbation with respect to the NIR laser. **b,** Quarter-cycle oscillations corresponding to three-photon absorption pathways. The quarter-cycle oscillation of the np^{2-} absorption feature is consistent with the second-order perturbation theory. The oscillation peaks are shifted somewhat with respect to the features labeled in Fig. 1a and b due to the AC Stark shifts near zero delay.

The relative strengths of the half-cycle and quarter-cycle periodicities can be evaluated experimentally by taking the Fourier transform along the delay axis for every photon energy and comparing the strengths of the different oscillatory components. The normalized oscillation amplitudes of the half- and quarter-cycle oscillations for the data in Fig. 1b are plotted in Figs 4a and b, respectively, with the two- and three-photon absorption pathways responsible for the oscillations labeled.

Sub-cycle Ponderomotive Shifts

The ponderomotive energy is the quiver energy of an electron in a laser field, averaged over the laser cycle. For our purposes, the ponderomotive energy represents an effective "shift" of the ionization potential for an electron ionized into a laser-dressed continuum state. Previous work[5] has demonstrated that the energy levels of bound states exhibit a sub-cycle energy shift, which is caused by the sub-cycle AC Stark shift. When the dressing laser field is not resonant with any atomic transition frequency, the bound electron energy levels shift according to the square of the *instantaneous* field strength. The nonresonant condition can be met in two cases: (1) the dressing laser frequency is much smaller than the spacing between energy levels or (2) the dressing laser frequency is much larger than the spacing between energy levels. The first case represents the DC limit, whereas case (2) applies for Rydberg energy levels in atoms and was investigated in Ref. 5. However, this effect can be observed in absorption experiments only when the dressing laser intensity is high enough to substantially ionize the excited state population, giving the state an effectively short lifetime, since absorption is by definition a time-integrated process.

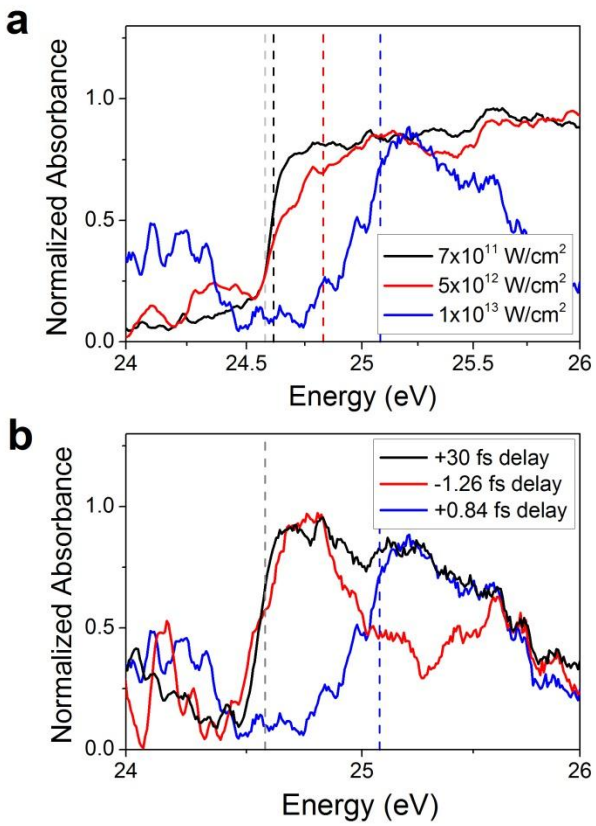

Fig. 5 | Ponderomotive energy shifts in the absorbance spectrum. a, Absorbance spectrum for different laser peak intensities at a fixed delay where the peak shift is maximal. The vertical dashed lines show the ionization potential I_p (24.58 eV, gray) and the ponderomotive shifted ionization potential I_p+U_p for dressing laser intensities of 7×10^{11} (black), 5×10^{12} (red), and 1×10^{13} W/cm^2 (blue). **b,** Absorbance spectrum for a laser peak intensity of 1×10^{13} W/cm^2 for different time delays. When the two pulses overlap, the absorption threshold shifts by approximately 0.5 eV.

The ponderomotive shift is the extension of the AC Stark shift into the continuum states, where the energy levels are infinitesimally spaced and condition (2) is therefore met perfectly. Furthermore, the time-resolved absorption process is not limited in resolution by long excited state lifetimes, as the electrons are already in the continuum. Therefore, the energy shift of the ionization threshold can in principle be measured with high fidelity. The delay-resolved absorption near the ionization potential (I_p = 24.58 eV) is shown in Fig. 3 of the main text. Here, we demonstrate that this absorption change is truly due to a shift of the ionization potential. Fig.

5a shows the measured absorbance at the maximum energy shifts for the dressing laser intensities of 7×10^{11}, 5×10^{12}, and 1×10^{13} W/cm^2, along with the corresponding ponderomotive-shifted ionization potential. In Fig. 5b, we show the measured absorbance for the intensity of 10^{13} W/cm^2 measured for three different values of the time delay. For a delay of 0.84 *fs*, we observe a maximum energy shift whereas the shift is minimal at a delay of -1.26 *fs*. These delays are separated by an odd number of laser quarter-cycles. We compare the absorbance at these delays with that at 30 *fs* delay, where no energy shift is observed. While the absorption threshold can be found at the ionization potential for the delays of 30 *fs* and -1.26 *fs*, it is shifted by approximately 0.5 eV at 0.84 *fs*.

References

1. Chu, S. I. & Reinhardt, W. P. Intense Field Multiphoton Ionization via Complex Dressed States: Application to the H Atom. *Phys. Rev. Lett.* **39**, 1195 (1977).
2. Chu, S. I. & Telnov, D. A. Beyond the Floquet theorem: generalized Floquet formalisms and quasienergy methods for atomic and molecular multiphoton processes in intense laser fields. *Phys. Rep.* **390**, 1 (2004).
3. Laughlin, C. & Chu, S. I. (in preparation)
4. Telnov, D. A. & Chu, S. I. High-order perturbation expansion of non-Hermitian Floquet theory for multiphoton and above-threshold ionization processes. *Phys. Rev. A* **61**, 013408 (1999).
5. Chini, M. *et al.* Delay control in attosecond pump-probe experiments. *Opt. Exp.* **17**, 21459 (2009).